Vacancy hardening in single-crystal $TiN_x(001)$ layers

C.-S. Shin, D. Gall,[a] N. Hellgren, J. Patscheider,[b] I. Petrov, and J. E. Greene
Department of Materials Science and the Materials Research Laboratory, University of Illinois, 104 South Goodwin, Urbana, Illinois 61801

(Received 12 December 2002; accepted 27 February 2003)

We investigate the effect of N vacancies on the mechanical properties of epitaxial δ-$TiN_x(001)$ layers with $x=0.67-1.0$. The relaxed lattice parameter increases linearly with x in good agreement with *ab initio* density functional calculations, indicating that deviations from stoichiometry are entirely due to anion vacancies. Hardness values increase continuously, while the elastic modulus decreases with increasing N-vacancy concentration. We attribute the observed vacancy hardening to a reduced dislocation mobility arising from an increase in the rate-limiting activation energy for cation migration. © *2003 American Institute of Physics.* [DOI: 10.1063/1.1568521]

I. INTRODUCTION

NaCl-structure δ-TiN_x thin films are widely used as hard, wear-resistant coatings on cutting tools, as diffusion barriers in microelectronic devices, and as corrosion- and abrasion-resistant layers on optical components. Experimental investigations of polycrystalline δ-TiN_x, which has a wide single-phase field extending from $x\simeq 0.6$ to $\simeq 1.2$,[1] show that optical, electronic, and mechanical properties vary as a function of x due to changes in bonding structure, charge carrier density, and microstructure.[2]

The effect of N vacancies on the mechanical properties of TiN_x has been controversial. The hardness (H) of polycrystalline TiN_x layers, grown by reactive magnetron sputtering, has been shown to increase with decreasing x.[3] However, the opposite behavior has also been reported for both bulk[4] and sputter-deposited[1,5] TiN_x. The differences arise primarily from large variations in layer microstructures including average grain size, grain size distribution, texture, density, and strain state. Reported hardness values are therefore not only a function of x, but also of the microstructure which depends, in turn, on growth and processing parameters. Using first-principles density functional methods, Jhi *et al.*[6] found that the shear modulus of TiN_x decreases with decreasing x. They concluded, based upon this result, that N vacancies reduce the hardness of substoichiometric TiN_x.

In this article, we circumvent the just-described experimental uncertainties related to film microstructure in determining $H(x)$ for δ-$TiN_x(001)$ by growing fully dense, epitaxial layers with $0.67\leqslant x\leqslant 1.00$. A combination of high-resolution reciprocal lattice mapping (HR-RLM) and *ab initio* density functional calculations establish that the deviation from stoichiometry is entirely due to N vacancies, and nanoindentation measurements show that the hardness H of $TiN_x(001)$ films increases continuously, while the elastic modulus E decreases, with decreasing x. For $TiN_{0.67}(001)$, H is $\simeq 50\%$ higher than that of TiN(001), while E is $\simeq 20\%$ smaller. We attribute the observed vacancy hardening to a reduced dislocation mobility arising from an increase in the rate-limiting activation energy for cation migration.

[a]Electronic mail: galld@rpi.edu
[b]Also at: Swiss Federal Laboratories for Material Testing and Research Überlandstrasse 129, CH-8600 Dübendorf, Switzerland.

II. EXPERIMENTAL PROCEDURE

All $TiN_x(001)$ layers were epitaxially grown at 700 °C to a thickness of 2600 Å on MgO(001) substrates in an ultrahigh vacuum (UHV) dc magnetron sputter deposition system described in Ref. 7. The target was a 7.6-cm-diam, 99.997% pure Ti disk, and sputtering was carried out at a total pressure of 20 mTorr (2.67 Pa) in mixed discharges consisting of Ar (purity = 99.9999%) and N_2 (99.999%), with N_2 fractions f_{N_2} between 0.027 and 1.0. The target current was 0.55 A, resulting in growth rates ranging from 380 Å-min^{-1} with $f_{N_2}=0.027$ to 86 Å-min^{-1} with $f_{N_2}=1.00$.

$TiN_x(001)$ layer compositions x were determined by Rutherford backscattering spectrometry (RBS) and the spectra analyzed using the RUMP simulation program.[8] The uncertainty in reported N/Ti ratios is less than ± 0.02. Film microstructures were investigated using a combination of high-resolution x-ray diffraction (HR-XRD), plan-view transmission electron microscopy (TEM), and cross-sectional TEM (XTEM). The XRD measurements were carried out in a high-resolution Philips MRD diffractometer with a Cu K_{α_1} source.

Nanoindentation responses of the $TiN_x(001)$ layers were determined using a Hysitron TriboScope™ instrument attached to an atomic force microscope. The triangular Berkovich diamond tip was calibrated using fused silica following the procedure described in Ref. 9. At least three indents were made in each sample using a multiple loading cycle with peak loads of 1, 2, 3, 5, 7, and 9 mN and unloading to 10% of the peak value between each loading. In the final unloading segment, a hold of 100 s was included at 10% of the peak load in order to allow system drift to be measured and corrected for. Hardness H and elastic modulus E values were determined from each unloading segment.

 © 2003 American Institute of Physics

Downloaded 14 May 2003 to 128.113.37.128. Redistribution subject to AIP license or copyright, see http://ojps.aip.org/japo/japcr.jsp

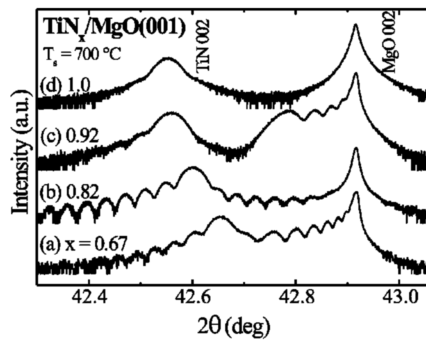

FIG. 1. HR-XRD ω–2θ scans from epitaxial δ-TiN_x layers grown on MgO(001) by UHV reactive magnetron sputter deposition at $T_s = 700\,°C$ in mixed N_2/Ar atmospheres with N_2 fractions f_{N_2}: (a) 0.027, (b) 0.030, (c) 0.032, and (d) 1.000.

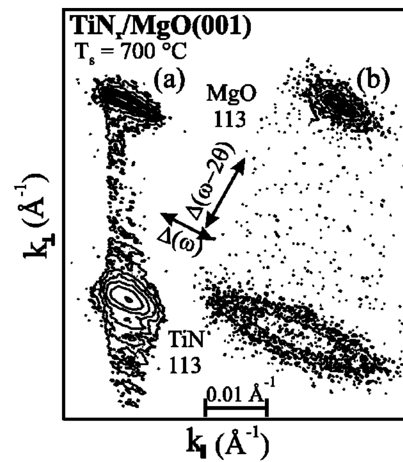

FIG. 2. HR-RLMs around the 113 reflection of epitaxial δ-TiN_x(001) layers grown at $T_s = 700\,°C$. (a) $x = 0.82$ and (b) $x = 1.0$.

III. RESULTS AND DISCUSSION

The combination of XRD, TEM, XTEM, and RBS analyses of the microstructure and composition of as-deposited layers as a function of f_{N_2} shows that films grown with $f_{N_2} = 0.027 - 1.0$ are single-crystal NaCl-structure δ-TiN_x(001) with a cube-on-cube epitaxial relationship to the substrate, $(001)_{TiN} \| (001)_{MgO}$ and $[100]_{TiN} \| [100]_{MgO}$, and N/Ti ratios $x = 0.67 - 1.00$.

The only detectable features in HR-XRD ω–2θ scans ($20° - 80°\ 2\theta$) from TiN_x/MgO(001) samples ($x \geqslant 0.67$) are the MgO 002 substrate peak at 42.915° ($a_{MgO} = 4.2112$ Å[10]) and the TiN_x 002 layer peak, which shifts to lower 2θ values with increasing f_{N_2}. Typical results for TiN_x layers with $x = 0.67$, 0.82, 0.92, and 1.00, grown with $f_{N_2} = 0.027$, 0.030, 0.032, and 1.000, respectively, are shown in Fig. 1. The TiN_x 002 peak position ranges from 42.654° for $x = 0.67$ ($f_{N_2} = 0.027$) to 42.560° for $x = 0.92$ ($f_{N_2} = 0.032$) due to corresponding changes in film composition and residual strain. For layers with $x = 1$ ($0.043 \leqslant f_{N_2} \leqslant 1.000$), the TiN 002 peak occurs at $2\theta = 42.552°$, yielding an out-of-plane lattice constant $a_\perp$ along the film growth direction of 4.2457 Å. In all cases, ω–2θ combined with ϕ-scan XRD results show that the layers are epitaxial, in agreement with TEM/XTEM analyses.

Finite-thickness interference fringes, clearly visible in HR-XRD scans from all substoichiometric TiN_x(001) layers, indicate that the films are of high structural quality with smooth surfaces and laterally uniform substrate/film interfaces. We attribute the higher crystalline quality of understoichiometric layers, compared to the stoichiometric TiN(001) layers, for which no interference fringes are obtained, to an increased cation surface mobility during growth under N-deficient conditions. From the fringe spacing, we obtain layer thicknesses in very good agreement with values from deposition rate calibrations.

Typical HR-RLMs about the asymmetric 113 reflection are shown in Fig. 2 for TiN_x(001) layers, with $x = 0.82$ and 1.0. Diffracted intensity distributions are plotted as isointensity contours as a function of the reciprocal lattice vectors $k_\|$ parallel and $k_\perp$ perpendicular to the surface. The in-plane $a_\|$, out-of-plane $a_\perp$, and relaxed a_o lattice parameters, as well as the in-plane strain $\varepsilon_\|$ and stress σ were determined as a function of x from the HR-RLM results and are listed in Table I. For the 113 reflection from an 001-oriented NaCl-structure sample, $a_\| = \sqrt{2}/k_\|$ and $a_\perp = 3/k_\perp$.

The fact that the substrate and layer peaks for the $x = 0.82$ sample [Fig. 2(a)] are aligned along $k_\|$ to within the instrument detection limit of $\simeq 2 \times 10^{-5}$ indicates that the film is fully strained. Corresponding measurements show that all understoichiometric ($x \leqslant 0.92$) TiN_x(001) layers are also fully coherent with the MgO(001) substrate. In contrast, substrate and layer peaks in the HR-RLM from the $x = 1$ layer in Fig. 2(b) are misaligned along $k_\|$, revealing the presence of in-plane strain relaxation due to misfit dislocations. The residual strain of stoichiometric layers, $\varepsilon_\| = -0.26\%$, can be fully accounted for by differential thermal contraction during sample cooling following deposition at 700 °C. The thermal expansion coefficients of TiN and MgO are 9.35×10^{-6} K^{-1}[11] and 1.3×10^{-5} K^{-1},[12] resulting in a thermal strain of -0.27% which is identical, within experimental uncertainty, to the measured strain. Thus, understoichiometric layers are fully strained with no detectable misfit dislocations and stoichiometric layers are fully relaxed at the growth temperature. This difference can be partially attributed to the lattice mismatch $\Delta a = (a_o - a_{MgO})/a_{MgO}$ at $T_s = 700\,°C$, which is 0.43% at $x = 1.00$ but decreases with increasing anion vacancy concentration to 0.10% at $x = 0.67$, thus reducing the driving force for the nucleation of misfit dislocations.

TABLE I. In-plane $a_\|$, out-of-plane $a_\perp$, and relaxed a_o lattice parameters, as well as the in-plane strain $\varepsilon_\|$ and stress σ of epitaxial TiN_x(001) layers versus film composition x. The film/substrate lattice misfit $\Delta a(a_{MgO} - a_{TiN}/a_{MgO})$ is also listed. RT is room temperature.

	$TiN_{0.67}$	$TiN_{0.82}$	$TiN_{0.92}$	$TiN_{1.0}$
$a_\|$ (Å)	4.2099	4.2126	4.2095	4.2289
$a_\perp$ (Å)	4.2345	4.2406	4.2467	4.2458
a_o (Å) at RT	4.2256	4.2305	4.2333	4.2397
a_o (Å) at 700 °C	4.2525	4.2574	4.2602	4.2667
$\varepsilon_\|$ (%)	−0.37	−0.42	−0.57	−0.26
σ(GPa)	−1.67	−1.89	−2.54	−1.17
Δa (%) at RT	−0.34	−0.46	−0.53	−0.68

Downloaded 14 May 2003 to 128.113.37.128. Redistribution subject to AIP license or copyright, see http://ojps.aip.org/japo/japcr.jsp

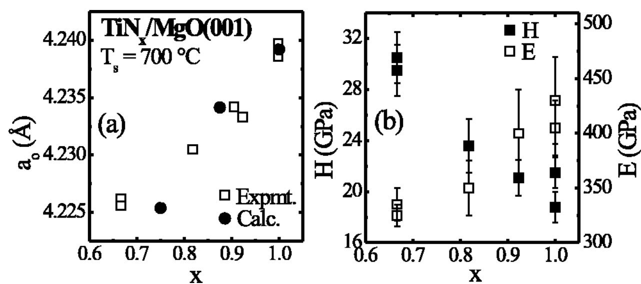

FIG. 3. (a) Relaxed lattice constants a_o determined from HR-RLMs of epitaxial TiN_x layers grown on MgO(001) at $T_s = 700\,°C$ and from *ab initio* calculations as a function of x. (b) Hardness (H) and elastic modulus (E) values vs x.

For $TiN_x(001)$ layers, a_o values are determined from $a_\parallel$ and $a_\perp$ results through the relationship $a_o = a_\perp[1-2\nu(a_\perp - a_\parallel)/a_\perp(1+\nu)]$, where $\nu = 0.22$ is the Poisson ratio of TiN.[13] Figure 3(a) is a plot of a_o versus x, where $a_o(x)$ increases approximately linearly from 4.2256 Å with $x = 0.67$ to 4.2333 Å with $x = 0.92$ and reaches 4.2397 Å at $x = 1.00$. Our $a_o(x)$ results for understoichiometric $TiN_x(001)$ layers are in good agreement with published values for bulk polycrystalline TiN_x samples,[14] as well as with reported results from N-implanted epitaxial Ti layers.[15]

In order to establish that the measured change in a_o as a function of x is due to the presence of N vacancies, we performed *ab initio* density functional calculations using the Vienna *ab initio* simulation package (VASP)[16] with the generalized gradient approximation (GGA) of Perdew and Wang.[17] Sixteen-atom supercells containing 0, 1, and 2 N vacancies were relaxed using a conjugate-gradient algorithm. a_o values for TiN, $TiN_{0.875}$, and $TiN_{0.75}$ were then determined by fitting the calculated total energies versus lattice parameters using the Murnaghan equation of state.[18] The calculated a_o values were reduced by a factor of 0.995 to account for the GGA bond length overestimation such that calculated and experimental values agree for stoichiometric TiN. The solid circles in Fig. 3, calculated a_o results for TiN_x, are in good agreement with the experimental data indicating that the deviation from stoichiometry is in fact due to N vacancies.

Hardness and elastic modulus values for $TiN_x(001)$ layers were determined from nanoindentation measurements carried out as described in Ref. 9. The results are plotted as a function of x in Fig. 3(b). For stoichiometric TiN(001), E is 430 ± 30 GPa, in good agreement with the previously reported value of 445 ± 38 GPa.[19] E continuously decreases with increasing N-vacancy concentration to 330 ± 20 GPa with $x = 0.67$. A similar reduction in E has been reported for strained polycrystalline TiN_x films.[20] E decreases since the N concentration is reduced with no change in crystal structure, while the bond lengths remain essentially constant. The high crystalline quality of understoichiometric $TiN_x(001)$ layers, as evidenced by the HR-XRD scans in Fig. 1, indicates that the Ti sublattice remains intact over the entire composition range, $0.67 \leq x \leq 1.00$. The average Ti–N bond length decreases by less than 0.4% as x is reduced from 1.00 to 0.67. Therefore, the primary effect of N vacancies is to reduce the Ti–N bond density, which is linear in x. A linear extrapolation of our $E(x)$ values to $x = 0$ [corresponding to fcc-Ti(001)] leads to a value of $\simeq 140$ GPa, which is close to the reported E value for hcp Ti, 120 GPa.[21] Thus, our results indicate that TiN_x gradually adopts the elastic properties of metallic Ti as the N content is reduced.

Figure 3(b) shows that $H(x)$ for TiN_x, in distinct contrast to $E(x)$, continuously increases with decreasing N concentration from 20.2 ± 2 GPa with $x = 1.00$ to 30 ± 2 GPa with $x = 0.67$. Materials exhibiting opposing dependencies in E and H versus composition are rare. In the present case, it indicates that while N vacancies reduce the resistance of TiN_x to reversible elastic deformation, they simultaneously increase the resistance to plastic deformation. Thus, it is clear that the enhancement in $H(x)$ is not due to strain hardening since this would also increase $E(x)$. Moreover, the measured room-temperature strain (see Table 1), with its highest value at an intermediate composition ($x = 0.92$), does not follow the composition dependence of H. We propose, therefore, that the increase in H with decreasing x is directly due to the presence of N vacancies in TiN_x. That is, $TiN_x(001)$ exhibits vacancy hardening.

We note that vacancy hardening is at odds with the conclusions by Jhi *et al.*[6] who found that the shear modulus G of TiN_x, calculated by density functional methods, decreases with decreasing x and, by assuming that $H \propto G$, proposed that $H(x)$ decreases with increasing N-vacancy concentration. Our results indicate that the assumption $H \propto G$ is not valid for understoichiometric TiN_x containing randomly distributed point defects (N vacancies).

Hardness, a measure of a material's resistance to the nucleation and glide of dislocations, is commonly observed in metals to increase with increasing point-defect concentrations due to dislocation pinning at the defect sites.[22] Thus, the increase in H that we measure with decreasing x in $TiN_x(001)$ suggests that the presence of N vacancies increases the dislocation formation energy and/or decreases the dislocation mobility. This is also consistent with our HR-XRD results showing that none of the substoichiometric $TiN_x(001)$ layers contain misfit dislocations, while stoichiometric TiN(001) layers are fully relaxed at the growth temperature. Dislocation migration requires a large number of individual cation diffusion hops between neighboring sublattice sites. The energy barrier E_h for such a hop is, in the case of stoichiometric samples, equal for all bulk lattice sites ($E_h = E_o$). However, in the presence of N vacancies, E_h is dependent on the local bonding environments at both initial and final sites.

In stoichiometric TiN(001), each Ti atom forms six Ti–N bonds along $\langle 100 \rangle$ directions. Since the primary slip system in TiN is the glide of $\langle 001 \rangle$ dislocations with Burgers vector $\mathbf{b} = a_o/\sqrt{2}\ \langle 011 \rangle$ on $\{110\}$ planes, migration of cations from the initial site to a nearest-neighbor site along $\langle 011 \rangle$ requires breaking four bonds, while the remaining two Ti–N bonds rotate during the migration. In the presence of a N vacancy, there are initially only five bonds, which, however, are slightly stronger on average than in stoichiometric TiN.[6] Depending on the location of the vacancy, either three or four bonds are broken, while two or one bond(s) remain, respectively. In the former case, $E_h < E_o$, since there is one less

Downloaded 14 May 2003 to 128.113.37.128. Redistribution subject to AIP license or copyright, see http://ojps.aip.org/japo/japcr.jsp

bond to break while in the latter case, $E_h > E_o$ due to the increased strength of the initial four bonds in the presence of the vacancy. Additional N vacancies at initial or final sites further broaden the range of E_h values.

Thus, understoichiometric TiN_x exhibits E_h values, dependent on the local environment of the migrating cation, which are both larger and smaller than E_o. Since cation hopping probabilities are proportional to $\exp(-E_h/kT)$, dislocation movement is limited by the largest E_h values. An increasing N-vacancy concentration leads to a wider distribution of E_h values and consequently to a higher activation barrier for dislocation migration and formation. This, in turn, results in the observed vacancy hardening effect.

IV. CONCLUSIONS

The opposing effects of N vacancies in $TiN_x(001)$ on $E(x)$ and $H(x)$ derive from the fundamental difference between elastic and plastic deformation. During elastic deformation, all interatomic bonds are strained simultaneously. Thus, E is a measure of the average bond strength multiplied by the bond density. $E(x)$ decreases with increasing N-vacancy concentration as the bond density decreases, with little variation in the average bond strength. In contrast, plastic deformation occurs due to a series of individual atom migration steps, which involve bond breaking and formation. N vacancies affect the local bond environment of migrating cations, causing variations in energy barriers for individual diffusion hops, which result in a rate-limiting value of $E_h > E_o$, thus decreasing dislocation mobility and, hence, increasing the hardness.

ACKNOWLEDGMENTS

This research was supported by the U.S. Department of Energy (DOE), Division of Materials Science, under Grant No. DEFG02-91ER45439 through the University of Illinois Frederick Seitz Materials Research Laboratory (FS-MRL). We also appreciate the use of the Center for Microanalysis of Materials at FS-MRL. Two of the authors (C. S. S. and N. H.) are partially supported by Hynix Semiconductor Inc., Ichon, Korea and the Swedish Foundation for International Cooperation in Research and Higher Education (STINT), respectively.

[1] J.-E. Sundgren *et al.*, in *Physics and Chemistry of Protective Coatings*, edited by J. E. Greene, W. D. Sproul, and J. A. Thornton (American Institute of Physics, Melville, New York, 1986), Ser. 149, p. 95.

[2] P. E. Schmid, M. S. Sunage, and F. Levy, J. Vac. Sci. Technol. A **16**, 2870 (1998); J. H. Kang and K. J. Kim, J. Appl. Phys. **86**, 346 (1999); P. Patsalas and S. Logothetidis, *ibid.* **90**, 4725 (2001).

[3] J. Chevallier, J. P. Chabert, and J. Spitz, Thin Solid Films **80**, 263 (1981); M. K. Hibbs, B. O. Johansson, J.-E. Sundgren, and U. Helmersson, *ibid.* **122**, 115 (1984); J. Musil, S. Kadlec, J. Vyskočil, and V. Valvoda, *ibid.* **167**, 107 (1988).

[4] J.-E. Sundgren and H. T. G. Hentzell, J. Vac. Sci. Technol. A **4**, 2259 (1986), references therein.

[5] X. Jiang *et al.*, J. Appl. Phys. **69**, 3053 (1991); J. Kohlscheen, H. R. Stock, and P. Mayr, Surf. Coat. Technol. **120–121**, 740 (1999); H. Holleck, J. Vac. Sci. Technol. A **4**, 2661 (1986).

[6] S.-H. Jhi, S. G. Louie, M. L. Cohen, and J. Ihm, Phys. Rev. Lett. **86**, 3348 (2001).

[7] I. Petrov, F. Adibi, J. E. Greene, W. D. Sproul, and W.-D. Münz, J. Vac. Sci. Technol. A **10**, 3283 (1992).

[8] R. L. Doolittle, Nucl. Instrum. Methods Phys. Res. B **15**, 344 (1985).

[9] C.-S. Shin *et al.*, Appl. Phys. Lett. **75**, 3808 (1999), and references therein.

[10] *Inorganic Index to Powder Diffraction File* (Joint Committee on Powder Diffraction Standards, Swarthmore, PA, 1997): Card No. 45-0946.

[11] K. Aigner, W. Lengauer, D. Rafaja, and P. Ettmayer, J. Alloys Compd. **215**, 121 (1994).

[12] H. Landolt and R. Börnstein, *Numerical Data and Functional Relationships in Science and Technology, Group III* (Springer, Berlin, 1975), Vol. 7, Pt. b1, p. 27.

[13] J. A. Sue, Surf. Coat. Technol. **54/55**, 154 (1992).

[14] L. E. Toth, *Transition Metal Carbides and Nitrides* (Academic, New York, 1971), p. 87, and references therein.

[15] Y. Kasukabe *et al.*, J. Vac. Sci. Technol. A **16**, 3366 (1998).

[16] G. Kresse and J. Hafner, Phys. Rev. B **47**, 558 (1993); **49**, 14251 (1994); G. Kresse and J. Furthmüller, Comput. Mater. Sci. **6**, 15 (1996); Phys. Rev. B **54**, 11169 (1996).

[17] J. P. Perdew and Y. Wang, Phys. Rev. B **45**, 13244 (1992).

[18] F. D. Murnaghan, Proc. Natl. Acad. Sci. U.S.A. **30**, 244 (1944).

[19] H. Ljungcrantz *et al.*, J. Appl. Phys. **80**, 6725 (1996).

[20] M. E. O'Herin, R. H. Parrish, and W. C. Oliver, Thin Solid Films **181**, 357 (1989).

[21] Z. Trojanova, P. A. Maksiniyuk, and P. Lukac, Phys. Status Solidi A **143**, K75 (1994).

[22] D. Hull, *Introduction to dislocations* (Pergamon Press, New York, 1967), p. 225.

Downloaded 14 May 2003 to 128.113.37.128. Redistribution subject to AIP license or copyright, see http://ojps.aip.org/japo/japcr.jsp